Journal of Materials Research and Technology 36 (2025) 6377–6386

Contents lists available at ScienceDirect

Journal of Materials Research and Technology

journal homepage: www.elsevier.com/locate/jmrt

Combined effect of micro-alloying and enhanced pre-aging on the paint-bake response of an AA 6014 alloy

Meng Liu [a,b,*,1], Xiulei Li [a,c,1], Jingwei Zhao [a], Zhenshan Liu [a], Ting Chen [b], Feng Qian [d], Xingzhong Cao [e], Qianning Guo [f], Zi Yang [f], John Banhart [f], Pizhi Zhao [a,**]

[a] Chinalco Materials Application Research Institute Co., Ltd., 102209, Beijing, China
[b] Chongqing National Innovation Institute of Light Alloys Co., Ltd., 400039, Chongqing, China
[c] Beijing University of Science and Technology, 100083, Beijing, China
[d] Beijing Institute of Technology, 100081, Beijing, China
[e] The Chinese Academy of Science, 100049, Beijing, China
[f] Helmholtz-Zentrum Berlin für Materialien und Energie, 14109, Berlin, Germany

ARTICLE INFO

Handling editor: L Murr

Keywords:
Al–Mg–Si alloys
Vacancy
Micro-alloying
Enhanced pre-aging
Paint baking

ABSTRACT

An enhanced pre-aging (EPA) process for 6000 series aluminum alloy automotive sheets has been developed, utilizing a micro-alloying strategy combined with vacancy concentration control. This innovative approach enhances the paint bake (PB) response by up to 70 % without compromising other properties. Microstructural characterizations and analyses of aging precipitation were conducted using positron annihilation spectroscopy, differential scanning calorimetry, transmission electron microscopy, and vacancy kinetics simulations. The measurements reveal that Sn retains a high concentration of supersaturated quenched-in vacancies. During the short high-temperature spike aging (SA) treatment, these vacancies effectively promote nucleation and give rise to a favorable Mg/Si ratio within the clusters/nuclei. In the subsequent conventional pre-aging (PA), simultaneous growth of nuclei and formation of new PA clusters occur. During PB, excess vacancies trapped by Sn/Cu and some clusters are released. This release effectively promotes the transformation of clusters into β" phase precipitates with a higher number density, smaller volume, and more dispersed distribution. This transformation substantially enhances the PB strength increment.

1. Introduction

Automotive light-weighting achieves weight reduction while still meeting key vehicle requirements. It also enhances dynamic performance and enables energy conservation and emission reduction. Aluminum alloys have become one of the most promising lightweight materials due to their low density, high specific strength, corrosion resistance, and relatively low cost compared to titanium, magnesium, and carbon fiber. 6000 series Al–Mg–Si alloys supplied in state T4P, i.e., solution heat treated (SHT) + pre-aged (PA) + natural aged (NA), or T4, i.e., in the SHT + NA condition, exhibit low yield strength and ductility, good formability, and significant strength increase during paint baking (PB). Consequently, they are widely used for automotive body panels.

PA plays a crucial role in enhancing the performance of 6000 series aluminum alloy automotive sheets [1–4]. This is primarily rooted in two phenomena. On the one hand, PA inhibits subsequent NA [5], thereby ensuring good formability of the sheet material. During PA, a significant number of vacancies and solute atoms are consumed, markedly reducing the concentration of supersaturated solute atoms and vacancies within the matrix, thus mitigating the detrimental effects of NA [6]. On the other hand, PA promotes the formation of the β" phase during artificial aging, thus enhancing the paint-baking strength. Atomic clusters precipitated during PA serve as nuclei for the β" phase during artificial aging. During PA, a substantial number of precipitated clusters can directly transform into coherent, needle-like (pre-)β" phases during baking, thereby increasing the baking strength. In addition to the conventional low-temperature, long-time PA treatment, a high-temperature, short spike-ageing (SA) treatment can be inserted

* Corresponding author. Chinalco Materials Application Research Institute Co., Ltd., 102209, Beijing, China.
** Corresponding author.
E-mail addresses: meng_liu275@chinalco.com.cn (M. Liu), pizhi_zhao@chinalco.com.cn (P. Zhao).
[1] Equal contribution to this work.

https://doi.org/10.1016/j.jmrt.2025.04.191
Received 19 March 2025; Received in revised form 17 April 2025; Accepted 17 April 2025
Available online 18 April 2025

between solution heat treatment and PA to further enhance the PB response of 6000 series aluminum alloy automotive sheets [7]. This allows the material in the T4P state to possess equivalent yield strength, i.e., equivalent formability, while simultaneously achieving higher PB strength. Consequently, under conditions of equal strength, the light-weighting effect can be further expanded.

The addition of micro-alloying elements to an alloy can further enhance the room temperature storage stability and PB response of sheet material. In 1974, Muromachi et al. demonstrated the significant impact of trace amounts of Sn on the aging kinetics of Al–Mg–Si alloys [8]. Recently, Pogatscher et al. reported that the addition of approximately 100 ppm of Sn to a 6061 alloy could completely inhibit the clustering of solute atoms within an NA window of about two weeks [9]. This is primarily due to the high binding energy between Sn atoms and vacancies. At room temperature, vacancies that would typically bind with Si and Mg atoms and facilitate their diffusion are instead captured by Sn, thereby significantly suppressing the formation of Mg–Si NA clusters. Simultaneously, the supersaturation of solute atoms is maintained. At PB temperature, the binding between Sn atoms and vacancies is weakened and large number of vacancies released that assist in the nucleation and growth of precipitates, thereby enhancing the PB response. The addition of trace amounts of Cu to the alloy can also further increase the PB response [10–12]. Numerous studies have shown that trace additions of Cu to Al–Mg–Si alloys do not directly lead to the strengthening phases Q and Q′ during PB, but rather promote the formation of denser clusters and the β" phase.

Based on the aforementioned research foundation, it can be theoretically inferred that Enhanced PA (EPA) under dual-element micro-alloying conditions (Sn, Cu) should enable an extended control of vacancies, thereby comprehensively optimizing the aging kinetics of the alloy. However, current research and development efforts in both academia and industry primarily focus on two aspects. One is investigating the mechanisms of single-step conventional PA. The other is the impact of individual micro-alloying elements on PB performance. Research on the coupling of EPA with dual-element micro-alloying has not yet been initiated and its superimposed effects await verification. Additionally, two main challenges persist in the related mechanistic research: (1) The scientific issues involved in both the mechanism of EPA itself and its influence on subsequent natural (NA) and artificial aging (AA) are far more complex than currently recognized. Due to the low total alloy content and poor elemental contrast in most Al–Mg–Si alloys, conventional experimental methods cannot be utilized to perform in-situ observations of the rapidly evolving microstructure during the early stages of aging [13]. The dynamic characterization of the microstructure is extremely difficult, and analyzing the kinetic behavior of vacancies, which facilitate atomic diffusion, presents an even more formidable challenge. This is one of the critical reasons why, after nearly 80 years of research, the negative effects of NA on AA in Al–Mg–Si alloys have not been fundamentally resolved [6]. Therefore, a comprehensive approach, including indirect characterization methods such as positron annihilation techniques and direct observation tools like transmission electron microscopy should be employed to qualitatively and quantitatively study the related processes. This will reveal the fundamental interaction mechanisms among vacancies, atoms, and clusters under different aging conditions; (2) Although some of the mechanisms of Sn or Cu effect on vacancy kinetics and the nucleation and growth of atomic clusters during conventional aging and PB processes have been clarified [14,15], the mechanism becomes more complex when Sn and Cu coexist and are coupled with EPA. Various experimental methods and simulations must be utilized to fully understand the basic interactions among vacancies, solute atoms, and their clusters at different stages of EPA. This constitutes the primary objective of the present study.

2. Experiments

2.1. Sample preparation

The compositions of the alloys investigated in this study are presented in Table 1.

The alloy ingots were produced by direct chill (DC) casting. After face milling, the ingots underwent a two-step homogenization treatment: primary homogenization at 500 °C × 4 h, followed by secondary homogenization at 570 °C × 8 h. The homogenized ingots were directly hot-rolled to 6-mm thick plates and then cold-rolled to 2.5 mm and subjected to an intermediate annealing step at 485 °C × 30 s in a salt bath furnace. Subsequently, the annealed plates underwent a second cold rolling step to a final thickness of 1 mm. The cold-rolled sheets were solution heat treated at 570 °C × 30 s in a salt bath furnace and immediately quenched to room temperature. Within 5 min of quenching (i.e. after short natural ageing, NA), the solution heat-treated sheets were subjected to either conventional PA or EPA treatments. Conventional PA was conducted in an air furnace, while EPA involved a two-step process: the first step, spike aging (SA), was carried out in an oil bath, followed by immediate transfer to an air furnace for the PA step, i.e. EPA = SA + PA. The relevant parameters for these treatments are listed in Table 3. After a 7-day natural secondary aging (NSA, excluded from the discussion for simplicity) and a 2 % pre-tensile deformation, the sheets underwent a simulated PB process in an oil bath furnace at 185 °C × 20 min, as outlined in Table 2.

2.2. Tensile test

The tensile properties of all pre-aged alloys were evaluated using a SHIMADZU AG-Xplus 100 kN testing machine. Each tensile test specimen had a gauge length of 50 mm. Three samples were tested for each condition.

2.3. PALS

Positron Annihilation Lifetime Spectroscopy (PALS) experiments [16] were conducted to investigate vacancy dynamics in 6014 alloys in different heat treatment states. They were carried out at the Institute of High Energy Physics, Chinese Academy of Sciences. A radioactive ^{22}Na source of ~13 μCi activity was employed as a positron emitter. Two identical samples were placed on either side of the ^{22}Na source, forming a typical geometric "sandwich" configuration. The conventional positron annihilation lifetime spectrometer utilized a pair of BaF_2 scintillation detectors to detect the gamma rays released after nuclear decay and positron annihilation. The positron annihilation lifetime spectrum was measured at ~20 °C using a fast-slow coincidence technique [17]. 2 million events were counted to ensure statistical reliability. The software “LT 9.0” was used for spectrum analysis. The time resolution of the spectrometer was approximately 0.210 ns. Due to strong positron trapping the spectra could be fitted reasonably well by one lifetime component.

2.4. DSC

Differential scanning calorimetry (DSC) can provide crucial information related to phase transformations in alloys. Therefore, this method was employed to analyze the 6014 and 6014SnCu alloys subjected to different PA and EPA treatments. DSC was performed using a Netzsch 204 F1 differential scanning calorimeter to characterize the thermic behavior of the alloys [18–20]. After quenching, DSC specimens weighing approximately 64 mg were placed in the DSC chamber. The samples were heated from 0 to 400 °C at a constant heating rate of 10 K/min.

Table 1
Composition of the 6014 and 6014SnCu alloys investigated (wt.%).

Alloy	Si	Fe	Cu	Mn	Mg	Cr	Ti	Sn	Al
6014	0.61	0.17	0.06	0.13	0.63	–	0.03	–	Bal.
6014SnCu	0.62	0.18	0.20	0.13	0.66	0.04	0.03	108 ppm	Bal.

Table 2
Laboratory preparation process of the investigated alloys.

Homogenization		Hot Rolling	Cold Rolling	Annealing	Cold Rolling	SHT	PA/EPA	NSA	PB
Heating	Holding								
60 °C/h + 35 °C/h	500 °C × 4 h + 570 °C × 8 h	50 mm → 6 mm	2.5 mm	485 °C × 30 s	1 mm	570 °C × 60 s	Table 3	25 °C × 7 d	185 °C × 20 min

Table 3
PB strength of 6014 and 6014SnCu alloys after various PA/EPA treatments (PB: 185 °C × 20 min). Column "T4P" gives strength before PB, column "PB ($R_{p0.2}$)" after. $\Delta R_{p0.2}$ is the difference between the two, the actual PB response.

Alloy	PA/EPA treatment		T4P	PB		
	1st step	2nd step	$R_{p0.2}$	$R_{p0.2}$	ΔPB	ΔPB
	(T/t)	(T/t)	(MPa)	(MPa)	(MPa)	(%)
6014	/	80 °C × 8h	106	204	98	48
	200 °C × 30s	80 °C × 8h	107	254	147	58
	200 °C × 30s	120 °C × 8h	183	280	97	35
6014SnCu	/	80 °C × 8h	98	243	145	60
	140 °C × 30s	80 °C × 8h	94	254	160	63
	170 °C × 30s	80 °C × 8h	94	254	160	63
	170 °C × 60s	80 °C × 8h	94	255	161	63
	170 °C × 120s	80 °C × 8h	94	259	165	64
	200°C × 30s	**80°C × 8h**	**95**	**260**	**166**	**63**
	200 °C × 60s	80 °C × 8h	96	253	157	62
	200 °C × 120s	80 °C × 8h	105	257	152	59
	170 °C × 30s	100 °C × 8h	117	266	149	56
	170 °C × 30s	120 °C × 2h	109	271	162	60
	170 °C × 30s	120 °C × 4h	142	276	134	49
	170 °C × 30s	120 °C × 8h	183	288	105	36
	200 °C × 30s	100 °C × 8h	123	270	147	54
	200 °C × 30s	120 °C × 2h	108	271	163	60
	200 °C × 30s	120 °C × 4h	139	280	141	50
	200 °C × 30s	120 °C × 8h	178	288	111	38

2.5. TEM

Thin foil specimens for transmission electron microscopy (TEM) were prepared using a Struers Tenupol-5 twin-jet electropolisher operated at ~20 V. The electropolishing solution consisted of 1/3 nitric acid (HNO_3) in methanol, maintained at a temperature of approximately −28 °C. Bright-field TEM images and quantitative analyses of precipitates were obtained using a JEOL 2100 microscope operated at an acceleration voltage of 200 kV. High-angle annular dark-field scanning transmission electron microscopy (HAADF-STEM) micrographs were acquired using a double aberration-corrected Thermo Fisher Themis Z TEM operated at 200 kV.

3. Results and discussion

3.1. Tensile tests

The 6014 and 6014SnCu alloys were subjected to conventional single-step PA and EPA processes, respectively. The PB response was then evaluated, as shown in Table 3.

The conventional 6014 alloy exhibits minimal differences in mechanical properties after various PA/EPA treatments. However, the PB strength is significantly improved (2nd row) following the enhanced PA process, resulting in a substantial increase in the PB response. Compared to single-step conventional PA, the EPA treatment at 200 °C × 30 s + 80 °C × 8 h results in a remarkable increase in PB strength to 254 MPa. Thus, the PB response increases from 98 MPa to 147 MPa, corresponding to a 50 % improvement, as shown in Fig. 1a.

The T4P strength of the 6014SnCu alloy is approximately 10 MPa lower than that of the conventional 6014 alloy. Notably, under single-step PA treatment, the PB response of the Sn and Cu micro-alloyed 6014 alloy (4th row) is comparable to that of the conventional 6014 alloy treated with EPA (2nd row). This indicates that the trace elements Sn and Cu can significantly enhance the PB response, achieving the same level as EPA. After the EPA treatment, the PB response of the 6014SnCu alloy further increases by 21 MPato 166 MPa (9th row). This demonstrates that EPA treatments are also applicable to Sn and Cu micro-alloyed 6014 alloys, although the increment of $R_{p0.2}$ is slightly reduced compared to the conventional 6014 alloy. To achieve the optimal effect of EPA, in addition to the optimization of homogenization and solution treatment processes mentioned above, it is crucial to properly match the corresponding aging temperature and time. The impact of the EPA process on the PB response was statistically analyzed, and the results are presented in Fig. 1b–d.

3.1.1. Impact of the first step high-temperature short-time SA on the PB response

Fig. 1b illustrates the influence of the SA temperature on the mechanical properties of the 6014SnCu alloy, with the SA time set at 30 s and the second-step PA schedule fixed at 80 °C × 8 h. As the SA temperature increases, the initial yield strength remains largely unaffected and is lower than that of the sample after PA only. Both the PB strength and the PB response gradually increase, surpassing those of the PA sample. This indicates that EPA also has a beneficial effect on improving the micro-alloyed 6014SnCu alloy. Furthermore, increasing the SA temperature contributes to further enhance the strengthening effect of EPA.

The impact of the SA time on the mechanical properties of the 6014SnCu alloy is also depicted in Fig. 1b, with the PA schedule fixed at 80 °C × 8 h. At an SA temperature of 170 °C, as the SA time increases, the initial T4P strength remains unchanged and lower than that of the conventional PA sample. Both the PB strength and the PB response gradually increase, surpassing those of the conventional PA schedule. This suggests that at an SA temperature of 170 °C, prolonging the SA time helps to further enhance the effectiveness of EPA. However, when the SA temperature is increased to 200 °C, the situation changes. As SA proceeds, the initial yield strength gradually increases. When the holding time exceeds 60 s, the initial yield strength surpasses that of the PA sample, indicating a decline in formability. The PB strength fluctuates, but the PB response gradually decreases, although it still remains higher than that of the conventional PA. Therefore, when the SA temperature is 200 °C, prolonging the holding time has an adverse effect.

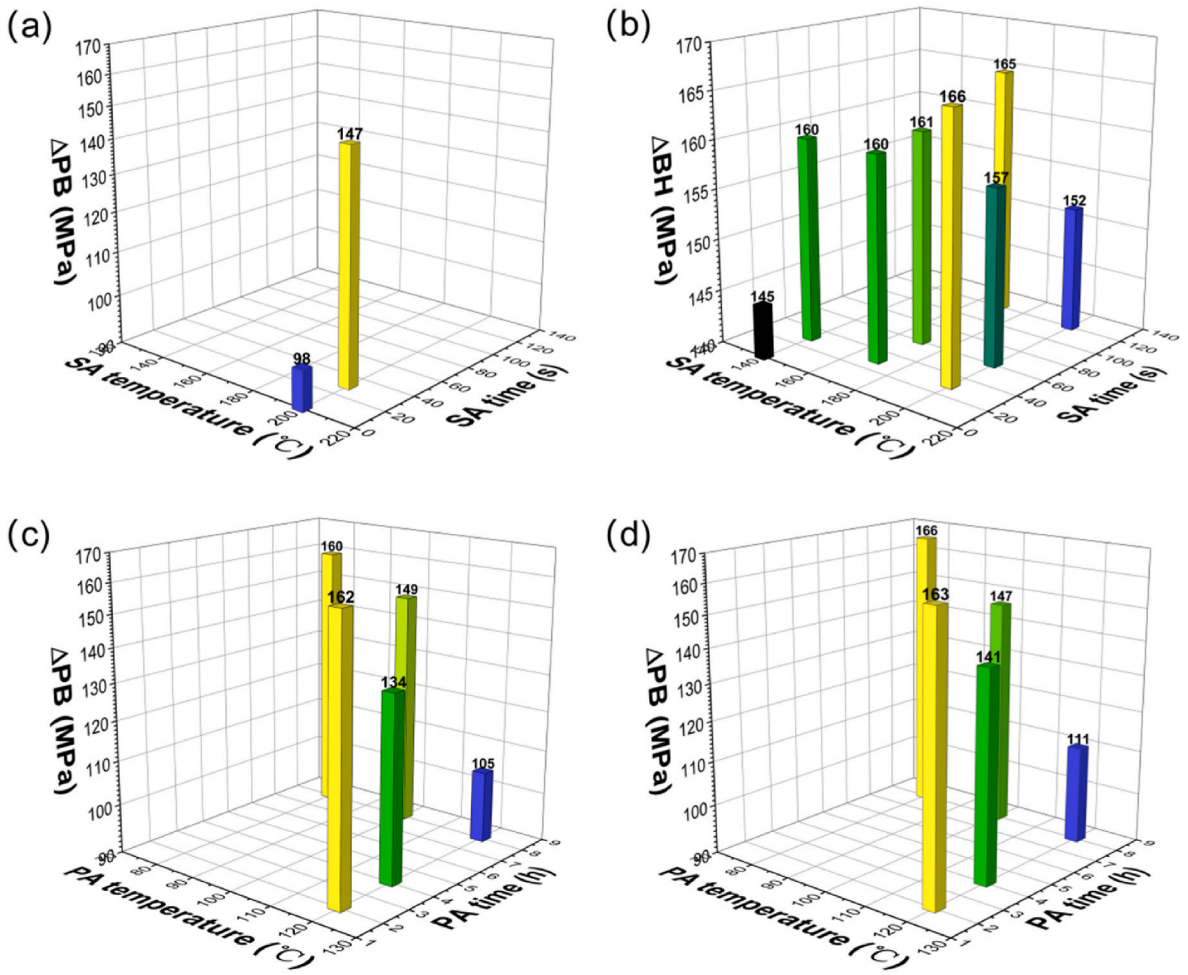

Fig. 1. The effect of SA/PA temperature and time on the PB response (same data as in Table 3): (a) 6014 alloy, with varying SA treatment and PA fixed at 80 °C × 8 h; (b) 6014SnCu alloy, with varying SA treatments and PA fixed at 80 °C × 8 h; (c) 6014SnCu alloy, with SA set at 170 °C × 30 s and varying PA treatments; (d) 6014SnCu alloy, with SA set at 200 °C × 30 s and varying PA treatments.

3.1.2. Impact of the second-step low-temperature long-time PA on the PB response

Subsequently, the influence of the second-step PA temperature on the properties of the 6014SnCu alloy is presented, with the PA time fixed at 8 h. As shown in Fig. 1c, when the first-step SA schedule is set to 170 °C × 30 s, an increase in the PA temperature leads to a sharp rise in the initial yield strength of the sheet, severely compromising its formability. Although the PB strength increases with the PA temperature, the PB response notably drops, indicating a significant reduction in the effectiveness of the EPA. A similar trend is observed when the SA schedule is 200 °C × 30 s, as depicted in Fig. 1d. This demonstrates that increasing the PA temperature has an extremely detrimental effect on the sheet properties.

Finally, the impact of the PA time on the properties of the 6014SnCu alloy is examined at a PA temperature of 120 °C. Similar to increasing the PA temperature, prolonging the PA time also has an adverse effect on the sheet properties. With the SA schedule set to 170 °C × 30 s, extending the PA time results in a sharp increase in the initial yield strength of the sheet, severely reducing its formability. Although the PB strength increases with the extension of the PA time, the PB response decreases sharply, as shown in Fig. 1c, indicating a significant reduction in the effectiveness of EPA. A similar trend is observed when the SA schedule is 200 °C × 30 s, as shown in Fig. 1d.

In summary, the addition of Sn and Cu can enhance the PB response of the 6014 alloy under conventional PA conditions, as the effect of EPA in the Sn/Cu-free 6014 alloy. The application of EPA can maximize the PB effect in the micro-alloyed 6014SnCu alloy, with a favorable PA schedule being 200 °C × 30 s + 80 °C × 8 h. Compared to conventional PA, this can further increase the PB response by 21 MPato 166 MPa.

3.2. MatCalc and PALS (vacancy dynamics)

3.2.1. MatCalc

MatCalc computations can provide useful information about the non-equilibrium vacancy concentrations in heat-treated aluminum alloys, utilizing the FSAK model [21]. Our prior calculations of the non-equilibrium vacancy concentration evolution during EPA (180 °C × 30 s + 85 °C × 8 h) and conventional PA (85 °C × 8 h) for alloy 6014 were referenced to facilitate the discourse on vacancy dynamics. These calculations are represented by the red and green curves, respectively, in Fig. 2.

The resulting vacancy concentration decreases at a much higher rate during EPA, particularly during the first SA stage compared to simple PA. This faster decrease is attributed to vacancy annihilation at sinks. This hypothesis is to be substantiated by PALS experiments, as detailed subsequently. Furthermore, the results suggest that after approximately 1 h (4×10^3 s, as depicted in Fig. 2) of PA at 85 °C, the vacancy concentrations for both cases approach the thermal equilibrium level. This is irrespective of the prior PA treatment history.

3.2.2. PALS

The results are presented together with our previous PALS

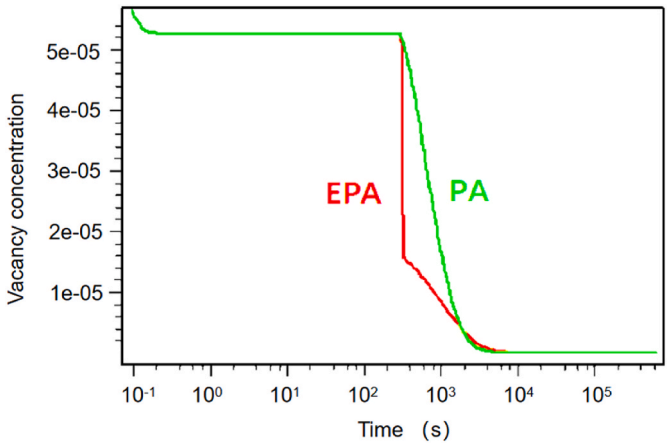

Fig. 2. Evolution of non-equilibrium vacancy concentration after solution treatment during PA + NSA (green) and EPA + NSA (red) processes as calculated by MatCalc.

measurements in a 6014 alloy [22] in Fig. 3. In the conventional 6014 alloy, the positron lifetime in vacancies is approximately 0.25 ns. In Mg–Si atomic clusters, it is about 0.215 ns, and in the aluminum matrix less than 0.16 ns [23]. As shown in Fig. 3, the measured positron lifetime that represents an average of various contributions in the as-quenched state is 0.23 ns. This is due to the preservation of a large number of non-equilibrium excess vacancies in the alloy after quenching. Under NA conditions, the lifetime decreases to the lowest point of its curve (gray open squares) after about 100 min. This indicates a significant reduction in excess vacancies and the formation of NA clusters with a lifetime of approximately 0.215 ns [17]. During annealing at 85 °C (PA), the lifetime decreases to its lowest point (0.21 ns, green open triangles) in just 1 min. This is also attributed to the disappearance of vacancies and the formation of PA clusters. It suggests that the precipitation kinetics of atoms are greatly accelerated at the PA temperature. During annealing at 200 °C (SA temperature) the disappearance rate of vacancies is even faster, with the positron lifetime almost reaching its lowest point (0.195 ns, red open triangles) within 30 s. This lifetime value is lower than the typical value for Mg–Si clusters (0.215 ns), but it does not decrease below the matrix lifetime (0.16 ns). This indicates that although SA clusters form, their size and/or number are insufficient to completely

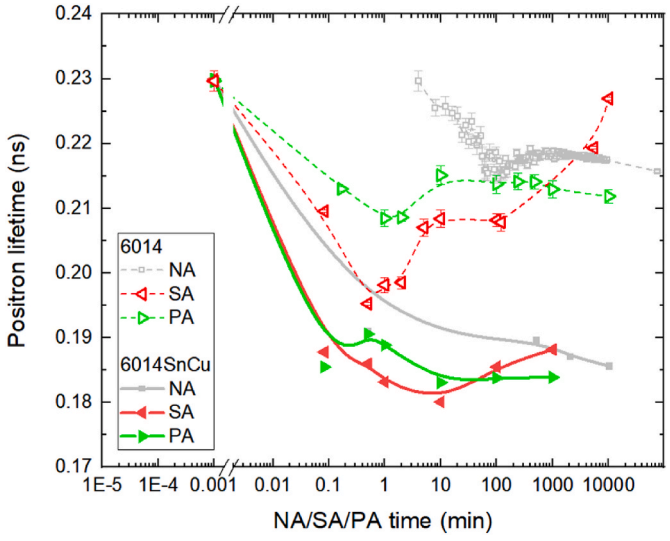

Fig. 3. Influence of treatments at PA (85 °C) and SA (200 °C) temperature on the one-component positron lifetime. The data for the Sn and Cu-free alloy is from Ref. [22]. Simple NA is included for comparison.

trap positrons. Thus, only a fraction of positrons annihilate in the matrix, resulting in a weighted average of positron lifetime between 0.16 and 0.215 ns. After reaching the lowest positron lifetime, all curves exhibit an upward trend, primarily due to the continuous formation and growth of clusters that increasingly trap positrons. In particular, the fraction of Si in the clusters gradually decreases, while Mg-rich clusters with a higher positron lifetime gradually become dominant [17].

For the 6014SnCu alloy under Sn and Cu micro-alloying conditions, although the evolution of positron lifetimes during different PA periods exhibits a consistent trend with the 6014 alloy, certain differences exist in the details.

The positron lifetime in the as-quenched state of the 6014SnCu alloy is also 0.23 ns. During NA, the positron lifetime continues to decrease but does not reach the lowest point until after 10000 min (gray solid squares) and might further decrease. This is primarily attributed to the high binding energy of Sn to vacancies (0.281 eV) compared to Mg and Si atoms during NA (see Table 5) [24]. In this case, the number of vacancies that could assist atomic diffusion is reduced, and the clustering of Mg and Si atoms is strongly suppressed, resulting in a deceleration of the aging kinetics. Additionally, the lowest lifetime (0.185 ns) is significantly lower than that of the 6014 alloy (0.215 ns). The binding energy calculations indicate a certain binding tendency between Mg–Si, Mg–Cu, and Mg–Sn atoms (see Table 5), suggesting a high likelihood of direct or indirect formation of Mg–Cu–Si–Sn clusters [25]. Apart from the contribution of the annihilated vacancies not captured by Sn atoms and the positron annihilation in the matrix due to limited clustering, Mg–Cu(–Si–Sn) clusters (with a lifetime of 0.185 ns for Cu–Mg clusters in the 2024 alloy) may be the primary cause of this lifetime value.

When the aging temperature is increased to 85 °C (green solid triangles) and 200 °C (red solid triangles), the positron lifetime in the 6014SnCu alloy exhibits the same decreasing trend as in the 6014 alloy. However, within 6 s, the rate of decrease is faster, and although it takes slightly longer (approximately 10 min) to reach the lowest lifetime value, the magnitude of the decrease is also greater compared to the 6014 alloy. Under SA and PA temperature conditions, the binding ability of Sn and Cu to vacancies is greatly weakened [26], allowing vacancies to diffuse more freely to sinks where they disappear. More importantly, these conditions facilitate the rapid formation of a certain amount of Mg–Cu(-*Si*-Sn) clusters/nucleation sites that capture positrons and the vacancies assisting their formation (based on Zurob's vacancy-pump model [27], see Discussion section 3.5) – the corresponding lifetime value reaches the minimum after 10 min. The rapid disappearance of vacancies observed by positrons during high-temperature PA is consistent with the Matcalc calculations shown in Fig. 2.

3.3. *DSC (clustering kinetics)*

The thermal traces of 6014 and 6014SnCu alloys after three different heat treatments are presented in Fig. 4.

For the as-quenched (AQ) state of the 6014 alloy, a distinct exothermic peak corresponding to the formation of NA clusters in the low-temperature range (~70 °C) is observed [28], as well as exothermic peaks associated with the formation of β" and β′ precipitates in the higher-temperature range (~250 °C, 300 °C) (black dashed line). After

Table 4
Measured average cross-sections, needle lengths, number densities, and volume fractions of precipitates in the two samples after 7 d NSA and 40 min PB.

Alloy	Cross-section A_p (nm^2)	Needle Length λ_p (nm)	Number Density N_p (m^{-3})	Volume Fraction f_p (%)
PA + NSA + PB	6.54	9.65	5.36×10^{22}	0.34
EPA + NSA + PB	6.12	8.20	1.62×10^{23}	0.81

Table 5
Calculated interaction energies (eV) for solute-solute [25] and vacancy-solute [15,24] complexes. Positive values correspond to attractive binding. The exact values may vary between different sources.

Solute-solute	Si–Si	Mg–Mg	Cu–Cu	Si–Mg	Sn–Sn	Si–Sn	Mg–Sn	Cu–Sn	Mg–Cu	Si–Cu
Interaction energy (eV)	−0.025	−0.037	−0.020	+0.042	n.a.	0	+0.1	+0.11	+0.043	−0.038
Vacancy-solute	V–Si	V–Mg	V–Sn	V–Cu						
Interaction energy (eV)	+0.033	+0.026	+0.281	+0.124						

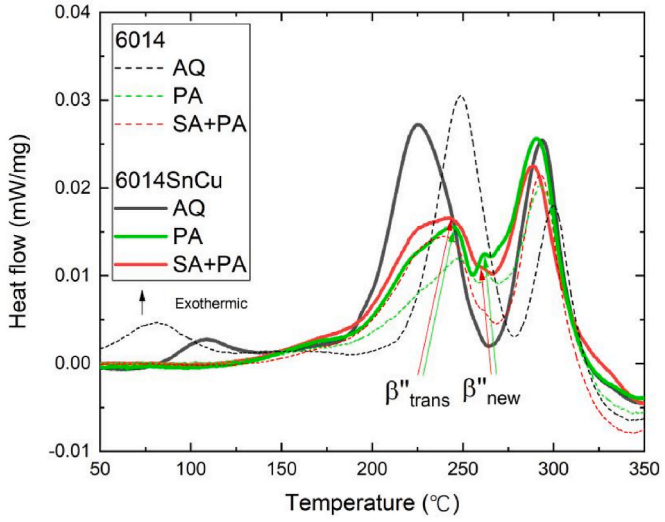

Fig. 4. DSC heat flow curves obtained after different PA and EPA (SA+PA) treatments. Data for the Sn and Cu free alloy is from Ref. [22].

conventional PA, the cluster peak disappears. This is due to the elimination of excess vacancies that drive clustering at these low temperatures. The β" precipitate peak dissociates into two sub-peaks, corresponding to the cluster transformation peak and a peak caused by formation of new clusters, respectively [19]. Compared to the AQ curve, the area under the β" peak is smaller due to the precipitation of some solute during PA. In the EPA curve, the two sub-peaks are also clearly visible, but the cluster transformation peak (left red dashed sub-peak) is shifted to a lower temperature of around 240 °C. Its area is larger than the corresponding sub-peak of conventional PA (left green dashed sub-peak). This suggests that the clusters formed during EPA are more prone to transform into the β" phase at higher temperatures, i.e. also during PB.

For the 6014SnCu alloy, the area of the low-temperature cluster peak decreases and the peak temperature increases, confirming the inhibitory effect of Sn and Cu on NA, with higher energy required for the formation of the clusters, mainly due to the higher temperature needed to dissociate the excess vacancies from the Sn atoms. In contrast, the temperature corresponding to the β" phase peak decreases by approximately 25 °C (black solid line) compared to the 6014 alloy. This is primarily due to the significant promotion of precipitate formation by Sn and Cu within the range of artificial aging temperatures. After conventional PA treatment, similar to the 6014 alloy, the NA peak disappears. This indicates that PA clusters can still precipitate during aging at the lower PA temperature while NA is simultaneously suppressed due to the annealing out of excess vacancies during PA. The β" precipitate peak also splits into two sub-peaks, corresponding to PA cluster transformation and formation of new clusters as for 6014. The dominant $\beta"_{trans}$ peak corresponds to a temperature similar to that of the 6014 alloy, but its area is significantly increased (left green solid line peak), comparable to the $\beta"_{trans}$ peak during EPA (left red dashed line peak). This suggests that under the condition of complex micro-alloying, even with the traditional single-step PA process, the efficiency of cluster transformation and the corresponding increment in PB strength are sufficiently high. This observation is consistent with the findings mentioned in section 3.1, where the PB response of the 6014SnCu alloy is comparable to that of the conventional 6014 alloy treated with EPA. Furthermore, the disappearance of the cluster peak and the two sub-peaks of the β" precipitate peak can also be observed in the 6014SnCu alloy prepared by EPA. The $\beta"_{trans}$ peak even shows a further decomposition characteristic (seen as a plateau at the top of the red solid line peak). The temperature corresponding to the leftmost peak decreases to approximately 220 °C, with an increased area compared to conventional PA. This indicates that clusters precipitated during EPA are more likely to transform into the β" phase during PB.

Based on the similar trends exhibited by the AQ, PA, and EPA curves of the 6014 and 6014SnCu alloys, it can be reasonably inferred that EPA plays a similar role in improving PB strength in the two alloys. However, the beneficial effect is amplified by the presence of Sn and Cu. This inference requires further validation through TEM as presented below.

3.4. TEM (precipitation morphology)

TEM was employed to visualize precipitates following PB treatment after conventional PA(+NSA) and EPA(+NSA) in the 6014SnCu alloy, as illustrated in Fig. 5. To enhance contrast and facilitate quantitative analysis, samples underwent an intentionally extended PB treatment (40 min) to amplify differences in precipitated phases. All TEM images were captured along the <100>Al zone axes. The investigation revealed that the EPA + NSA + PB sample exhibits smaller but more densely distributed phases compared to the PA + NSA + PB sample.

Quantitative analysis was conducted in the following in the same way as in Ref. [22] to determine the number density (N_p), average length (λ_p), and average cross-sectional area (A_p) of precipitates. The number density of needle-like precipitates was calculated using the formula $N_p = \frac{3N}{A(\lambda_p+t)}$, where N represents the count of precipitate cross-sections within the image area (A) as viewed in the observation direction, and t is the estimated thickness of the TEM foil determined by convergent beam electron diffraction (CBED) [29]. A minimum of four images was analyzed for each sample. The quantified parameters of the precipitates are presented in Table 4, including cross-sections, needle lengths, number densities, and volume fractions.

For the calculation of the yield strength model, three dominating contributions were considered [30–33]:

$$\sigma_y = \sigma_i + \sigma_{ss} + \sigma_{par} \quad (1)$$

where σ_i, σ_{ss} and σ_{par} denote the contributions from the Al matrix (with a value of 10 MPa [32,34], noting that grain boundary strengthening is incorporated within σ_i), solid solution strengthening for the as-quenched material, and by the second-phase particles (as the predominant contribution), respectively. To simplify the calculation according to Eq. (1), we hypothesize that ΔPB is predominantly affected by σ_{par}, which can be expressed as [3,34–36]:

$$\sigma_{par} = \frac{M\beta Gbr^{1/2}}{r_c^{3/2}}\sqrt{\frac{6f_p}{\pi}} \quad (2)$$

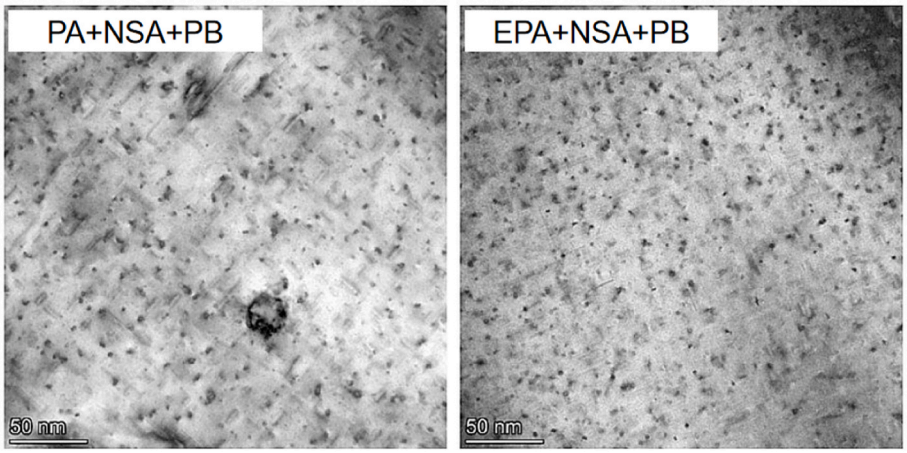

Fig. 5. Effect of different PA processes on precipitation phases during PB in 6014SnCu alloy.

where, M represents the Taylor factor, b the magnitude of the Burgers vector, β a geometric constant, and r and f_p the average radius and volume fraction of the particles, respectively. Assuming that G and r_c are comparable between the EPA and PA samples, the net strengthening contribution from particles primarily depends on the size of the particles and the volume fraction f_p.

Since parameters such as r_c in the above equation are not readily calculable but significantly influence σ_{par}, we attempt to calculate $\frac{\sigma_{par2}}{\sigma_{par1}}$ instead to ascertain the impact of SA on PB (the subscript "1″ refers to PA + NSA + PB and "2″ to EPA + NSA + PB). Assuming that the second-phase particles from both samples share the same structure, the following relationship can be established:

$$\frac{\sigma_{par2}}{\sigma_{par1}} = \left(\frac{r_2}{r_1}\frac{f_{p2}}{f_{p1}}\right)^{1/2} \tag{3}$$

where, the volume fraction f_p can be described by Ref. [3]:

$$f_p = \frac{3N}{A(t+\lambda_p)}A_p\lambda_p \tag{4}$$

Here, $\frac{3N}{A(\lambda_p+t)}$ denotes the number density N_p of the precipitates. Then, $\frac{\sigma_{par2}}{\sigma_{par1}}$ can be estimated accordingly by assuming that the precipitates are spherical with an equivalent radius r_i of the precipitates given by $\frac{4}{3}\pi r_i^3 = A_{pi}\lambda_{pi}$). Then,

$$\frac{\sigma_{par2}}{\sigma_{par1}} = \left(\frac{A_{p2}}{A_{p1}}\frac{\lambda_{p2}}{\lambda_{p1}}\right)^{2/3}\left(\frac{N_{p2}}{N_{p1}}\right)^{1/2} \tag{5}$$

Based on the statistical analysis of the TEM micrographs, $\frac{A_{p2}}{A_{p1}} = 0.94$, $\frac{\lambda_{p2}}{\lambda_{p1}} = 0.85$, $N_{p1} = 5.36\times 10^{22}$ m^{-3}, $N_{p2} = 1.62 \times 10^{23}$ m^{-3}, $\lambda_{p1} = 9.65$ nm, $\lambda_{p2} = 8.20$ nm, thus:

$$\frac{\sigma_{par2}}{\sigma_{par1}} \approx 1.50$$

Fig. 5 provides a rough estimate of the second-phase particle-related ratio of $\sigma_{par(SA+PA+NSA+PB)}/\sigma_{par(PA+NSA+PB)} \approx 1.50$. This value exceeds the ratio which can be derived from $R_{p0.2(SA+PA+NSA+PB)}/R_{p0.2(PA+NSA+PB)} \approx 1.07$ following 20 min PB as opposed to 40 min of PB (refer to Table 3. However, considering the additional 20 min of PB and potential calculation errors, both values exhibit a consistent trend. Hence, the higher bake hardening effect achieved by carrying out SA before PA can likely be attributed to the increased number density of small- and medium-sized precipitates. These impede dislocation movement via the shearing mechanism.

A representative HAADF-STEM micrograph of the sample subjected to EPA, 7 d NSA and 40 min PB is presented in Fig. 6. This image reveals needle-shaped precipitates with characteristic "eye" units (also termed "low density cylinders") in cross-section, formed within the Al matrix. Notably, several columns within the precipitate exhibit relatively high Z contrast, suggesting partial occupation by Sn and/or Cu atoms. Werinos et al. reported the presence of Sn not only in the matrix but also within precipitates in Sn-added AA6061 samples using APT [26]. This finding aligns with our HRTEM observations and indicates that small Sn precipitates can serve as heterogeneous nucleation sites.

3.5. Mechanism

3.5.1. Mechanism of EPA in 6014 alloy

EPA differs from conventional PA by the brief (5–30 s) high-temperature heating step. Despite this brief step, it notably improves the PB response. The core mechanism involves the interaction between vacancies, atoms, and their clusters during this process. SA involves heating a sample to approximately 170 °C within 10 s and holding at 180 °C for 20 s and essentially mirrors the initial stage of artificial aging. Consequently, the underlying mechanisms should be similar. While numerous studies have explored artificial aging mechanisms, few have focused on the very early stages (within 1 min), primarily due to limitations of in-situ characterization techniques. MatCalc calculations indicate that excess vacancy concentrations rapidly decrease during the 30-s SA period, regardless of whether vacancy-solute atom interactions are considered. Conventional PA requires significantly longer times to achieve comparable vacancy concentration levels. In-situ positron annihilation experiments corroborate these calculations. The rapid decrease in vacancy concentration can be attributed to two factors: (1) At higher temperatures, vacancies are more likely to diffuse to dislocations, grain boundaries, and surfaces, effectively "disappearing" [37]. (2) Vacancies may be permanently captured by sufficiently large clusters, leading to their "virtual disappearance." According to Zurob's model [27], vacancies initially combine with atoms to form complexes, transporting them to specific locations. They then dissociate with a probability corresponding to $\exp(ncE_b)$ before diffusing to the next solute atom. This process repeats, allowing atomic clusters to nucleate and grow until they are large enough to permanently trap vacancies at the given temperature [27]. The positron lifetime during the SA stage suggests the formation of "SA clusters". Without cluster formation, vacancies would rapidly disappear at defect sites, resulting in a positron lifetime below 0.165 ns. However, the observed 0.195 ns lifetime indicates a weighted average of SA clusters (~0.215 ns) and the matrix (<0.160 ns). It was proposed that these cluster-bound vacancies promote the formation of clusters with a more favorable energy

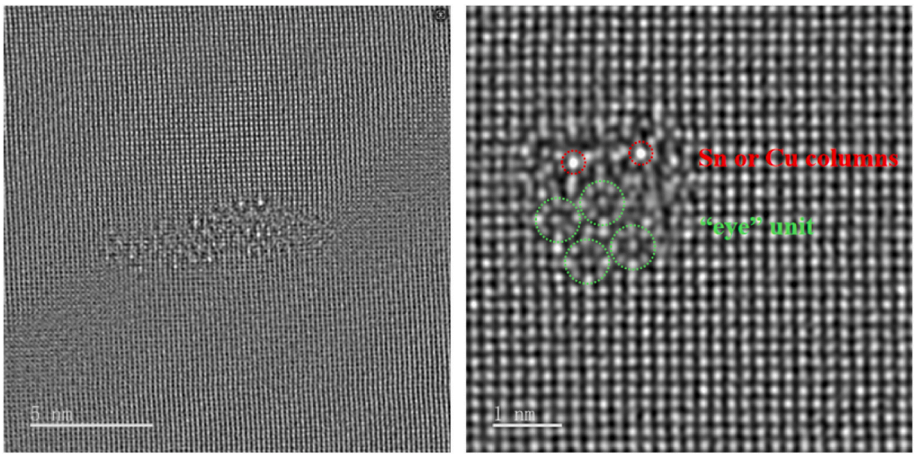

Fig. 6. HRTEM observation of precipitated phases in 6014SnCu alloy after EPA, NSA and 40 min PB.

configuration and a Mg/Si ratio close to 1 and facilitate their transformation into β" precipitates [38,39]. In contrast, conventional PA conditions result in a broader distribution of Mg/Si ratios in PA clusters due to a higher proportion of vacancies disappearing at sinks. From an atomic diffusion perspective, the diffusion abilities of Mg and Si atoms increase with temperature, with the difference between them narrowing. Compared to NA, PA consumes supersaturated vacancies and solute atoms to form clusters with a narrower Mg/Si ratio distribution, which are more stable and conducive to transformation during PB. The observation that the highest mechanical strength is achieved after quenching and direct PB suggests an important point. Clusters formed during high-temperature SA have Mg/Si ratios closer to 1 compared to those formed during lower-temperature PA. This proximity facilitates their transformation into the β" phase. A schematic illustration of this process is provided in Fig. 7.

The conventional low-temperature, long-duration PA treatment following SA serves two purposes. Firstly, it promotes the growth of the clusters grown during previous SA (at 200 °C) that are most conducive to transformation during PB. Secondly, it facilitates the formation of new PA clusters at 85 °C. During the final PB stage after a 7-day natural aging period, these clusters transform into the β" phase with a higher number density, resulting in a more pronounced increase in PB strength. This observation aligns with the DSC results, which show a larger area and lower temperature β" transformation peak corresponding to EPA.

3.5.2. *Mechanism of EPA in 6014SnCu alloy*

The experimental results presented in Sections 3.2-3.3 demonstrate that the EPA mechanism in the 6014SnCu alloy follows a similar trend to that of the 6014 alloy. However, certain differences exist, evidently caused by the introduction of Sn and Cu atoms. Therefore, it is necessary to further examine the influence of elements such as Sn at various aging stages.

To comprehend the effect of Sn on aging, it is crucial to consider the interaction energies between different elements and between vacancies and various elements. As shown in Table 5, the calculated binding energy between Mg and a vacancy is 0.026 eV, and slightly higher for Si at 0.033 eV. In contrast, the binding energy between a Sn atom and a vacancy increases by an order of magnitude to 0.281 eV. Consequently, the addition of Sn and Cu would increase the vacancy concentration after quenching according to the Lomer equation [40]:

$$\chi_v = \exp\left(\frac{S_f}{k_B}\right)\exp\left(-\frac{E_f}{k_BT}\right)\left[1-12\left(c_{Mg}+c_{Si}+c_{Sn}+c_{Cu}\right)+12\left[c_{Mg}\exp\left(\frac{E_{V-Mg}}{k_BT}\right)+c_{Si}\exp\left(\frac{E_{V-Si}}{k_BT}\right)+c_{Sn}\exp\left(\frac{E_{V-Sn}}{k_BT}\right)+c_{Cu}\exp\left(\frac{E_{V-Cu}}{k_BT}\right)\right]\right]. \quad (6)$$

However, Sn can also significantly inhibit NA through its strong binding to vacancy-type defects [41–43]. As the temperature rises, the binding effect on vacancies gradually diminishes as governed by an Arrhenius-type temperature dependency. Only when the aging temperature approaches or even exceeds 180 °C [44] does Sn gradually release the captured vacancies (or Sn-vacancy complexes), thereby promoting the diffusion of other solutes at these elevated temperatures to facilitate β" phase precipitation.

If the temperature is set to 180 °C, the addition of Sn alone results in sub-optimal strength after PB [44]. However, when a certain amount of

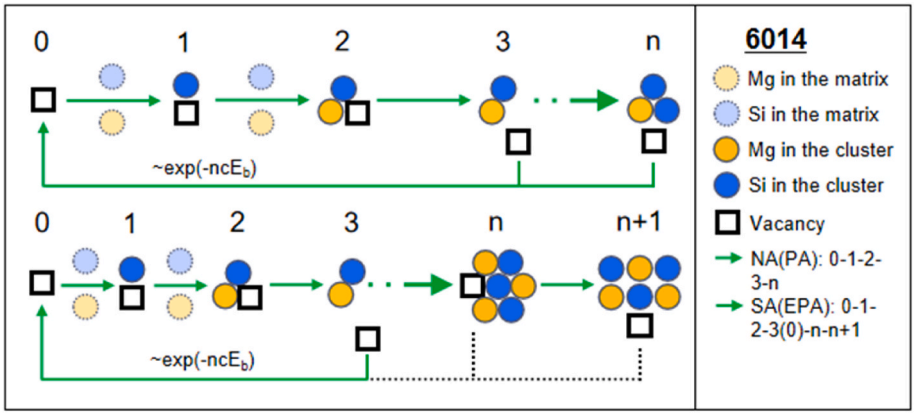

Fig. 7. Schematic diagram of the cluster formation mechanism in 6014 alloy.

Cu is added in conjunction with trace amounts of Sn, several effects are observed. Firstly, Cu itself provides solid solution strengthening. Secondly, at NA and PA temperatures, the binding between vacancies and Cu is weaker than that between vacancies and Sn, thus maintaining the Sn-dominated inhibitory effect. During PB, both Cu and Sn exhibit a greatly reduced ability to bind vacancies. At this temperature, Sn's inhibitory effect on aging transforms into a promotional one [44]. The previously retained vacancies are released, facilitating the efficient transformation of clusters into the β" phase. Simultaneously, other strengthening phases, such as the Cu-associated Q′ phase, can form rapidly (see Fig. 8).

As previously mentioned in section 3.5.1, vacancies bound to clusters can facilitate the formation of clusters with a more energetically favorable configuration and a Mg/Si ratio approaching 1. This ultimately promotes their transformation into β" precipitates [38]. The strong interactions between Sn, Cu, and their corresponding clusters with vacancies are further enhanced by EPA. This should result in a higher number of bound vacancies. This increased quantity of bound vacancies will enable a substantially larger number of (E)PA clusters to rapidly transform into β" strengthening phases during PB. This is compared to those treated with conventional single-step PA and PB in the 6014/6014SnCu alloys. Such phases are smaller in volume, which aligns with the observations from DSC and TEM analyses.

Therefore, the dual addition of specific amounts of micro-alloying elements Sn and Cu combined with EPA is complementary. This approach harnesses the effect of Sn and Cu in retaining vacancies at low temperatures, which are subsequently released during baking to promote precipitation. Simultaneously, it enhances the conversion of EPA clusters into the β" phase, thus achieving a synergistic effect. This strategy comprehensively optimizes the aging kinetics and overall mechanical properties of the alloy from both compositional and processing perspectives. Furthermore, as the strength of sheets prepared by both conventional and EPA continues to increase when the baking time is extended to 40 min, the strengthening mechanism can be attributed to the shear mechanism.

4. Conclusions

This study investigates the impact of extended pre-aging (EPA) under micro-alloying conditions on the paint-bake (PB) response of 6000 series alloys. EPA increases the PB response of the 6014 alloy notably. Under conventional PA conditions, the 6014SnCu alloy achieves a PB response comparable to that of the normal 6014 alloy after EPA. Applying EPA to the 6014SnCu alloy further improves the paint-bake effect. The precipitation kinetics of second-phase particles corresponding to different aging stages were analyzed using various microstructural characterization techniques. The dynamic characteristics of supersaturated vacancies were verified through simulation calculations. The main research findings are summarized as follows.

I. Mechanism of EPA in 6014 Alloy
- Despite the short spike-aging (SA) time, the interaction with excess vacancies significantly optimizes the kinetics of subsequent cluster and precipitate formation and markedly increase the alloy's PB response.
- Compared to conventional PA, during SA, excess vacancies not only diffuse to sinks but also facilitate rapid formation of SA clusters or nucleation sites at higher temperatures.
- During low-temperature aging, free vacancies and vacancy-solute complexes assist in cluster formation. According to the vacancy-pump model, as the cluster/particle size increases, the probability of vacancies escaping from clusters and assisting in the diffusion of another atom gradually decreases. This continues until they are "permanently" trapped by clusters exceeding the critical size. These "permanently" bound vacancies progressively optimize the cluster's energy configuration. They bring the Mg/Si ratio closer to 1, which is more favorable for later transformation.
- During subsequent PA, SA clusters continue to grow while new PA clusters form simultaneously.
- Ultimately, the higher density of transformable clusters formed after EPA leads to a denser β" precipitate phase distribution, thus significantly enhancing the PB response.

II. Mechanism of EPA in 6014SnCu Alloy
- The EPA mechanism in micro-alloyed 6014 alloy shares similarities with conventional 6014 but exhibits some distinct differences.
- Compared to Mg and Si, the introduction of Sn(Cu) results in more post-quench supersaturated vacancies. At room temperature, Sn atoms retain more vacancies through strong interactions.
- During SA, due to higher temperatures, the interaction between Sn atoms and vacancies weakens significantly. This allows vacancies previously bound by Sn atoms to rapidly assist in the formation of more Mg–Si clusters. Sn may also act as a heterogeneous nucleation site, accelerating the nucleation process and further increasing SA cluster density. After the ordering of solute atoms assisted by vacancies, clusters with Mg/Si ratios closer to the β" phase are more prevalent compared to the 6014 alloy.
- In subsequent aging, existing SA clusters continue to grow while new PA clusters form concurrently.
- During high-temperature PB, some previously bound vacancies are released. These re-released vacancies and their complexes with Sn atoms further promote the precipitation of more dispersed and finer β" phases, resulting in the maximum PB response.

From an industrial application perspective, to achieve the ultimate

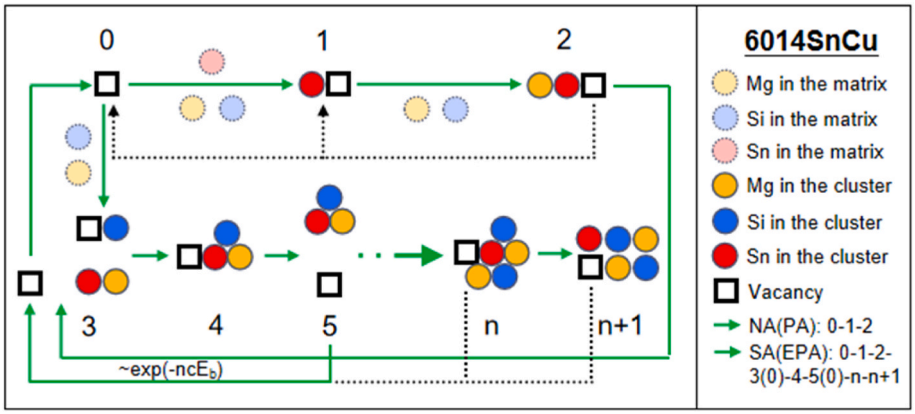

Fig. 8. Schematic diagram of the cluster formation mechanism in 6014SnCu alloy.

PB response, the micro-alloying + EPA approach is recommended. If a significant reduction in total PA time is required, the temperature of the second PA step can be appropriately increased. Additionally, the micro-alloying + traditional single-step PA approach can also significantly enhance the PB response.

Declaration of competing interest

The authors declare that they have no known competing financial interests or personal relationships that could have appeared to influence the work reported in this paper.

Acknowledgment

M. Liu gratefully acknowledges the financial support from the Beijing Natural Science Foundation (No. 2222095). Q.N. Guo would like to express thanks for the research fellowship (No. 201706050074) from the China Scholarship Council (CSC).

References

[1] Zhen L, Kang SB. The effect of pre-aging on microstructure and tensile properties of Al-Mg-Si alloys. Scripta Mater 1997;36:1089–94.
[2] Yang Z. Multi-stage ageing in an Al-Mg-Si alloy, (ph.D. Thesis). TU Berlin; 2019.
[3] Engler O, Marioara CD, Aruga Y, Kozuka M, Myhr OR. Effect of natural ageing or pre-ageing on the evolution of precipitate structure and strength during age hardening of Al–Mg–Si alloy AA 6016. Mater. Sci. Eng. A 2019;759:520–9.
[4] Birol Y. Pre-aging to improve bake hardening in a twin-roll cast Al-Mg-Si alloy. Mater. Sci. Eng. A 2005;391:175–80.
[5] Aruga Y, Kozuka M, Takaki Y, Sato T. Formation and reversion of clusters during natural aging and subsequent artificial aging in an Al-Mg-Si alloy. Mater. Sci. Eng. A 2015;631:86–96.
[6] Pashley DW, Rhodes JW, Sendorek A. Delayed ageing in aluminium-magnesium-silicon alloys: effect on structure and mechanical properties. J Inst Met 1966;94:41–9.
[7] Zandbergen MW, Xu Q, Cerezo A, Smith GDW. Study of precipitation in Al-Mg-Si alloys by atom probe tomography I. Microstructural changes as a function of ageing temperature. Acta Mater 2015;101:136–48.
[8] Muromachi S, Mae T, Al-1.3wt%Mg2Si. J. Jap. Ins. Met. Mater. 1974;38:130–8.
[9] Pogatscher S, Antrekowitsch H, Werinos M, Moszner F, Gerstl SSA, Francis MF, Curtin WA, Löffler JF, Uggowitzer PJ. Diffusion on demand to control precipitation aging: application to Al-Mg-Si alloys. Phys Rev Lett 2014;112:225701.
[10] Wenner S, Marioara CD, Andersen SJ, Holmestad R. Effect of room temperature storage time on precipitation in Al-Mg-Si(-Cu) alloys with different Mg/Si ratios. Int J Mater Res 2012;103:948–54.
[11] Morley AI, Zandbergen MW, Cerezo A, Smith GDW. The effect of pre-ageing and addition of copper on the precipitation behaviour in Al-Mg-Si alloys. Mater Sci Forum 2006;519–521:543–8.
[12] Kim JH, Marioara CD, Holmestad R, Kobayashi E, Sato T. Effects of Cu and Ag additions on age-hardening behavior during multi-step aging in Al-Mg-Si alloys. Mater. Sci. Eng. A 2013;560:154–62.
[13] Banhart J, Chang CST, Liang ZQ, Wanderka N, Lay MDH, Hill AJ. Natural aging in Al-Mg-Si alloys - a process of unexpected complexity. Adv Eng Mater 2010;12(7):559–71.
[14] Liu M, Zhang XP, Körner B, Elsayed M, Liang ZQ, Lezvraz D, Banhart J. Effect of Sn and in on the natural ageing kinetics of Al-Mg-Si alloys. Materialia 2019:100261.
[15] Liu M, Banhart J. Effect of Cu and Ge on solute clustering in Al-Mg-Si alloys. Mater. Sci. Eng. A 2016;658:238–45.
[16] Staab TEM, Krause-Rehberg R, Hornauer U, Zschech E. Study of artificial aging in AlMgSi (6061) and AlMgSiCu (6013) alloys by positron annihilation. J Mater Sci 2006;41:1059–66.
[17] Liu M, Čížek J, Chang CST, Banhart J. Early stages of solute clustering in an Al–Mg–Si alloy. Acta Mater 2015;91:355–64.
[18] Edwards GA, Stiller K, Dunlop GL, Couper MJ. The precipitation sequence in Al-Mg-Si alloys. Acta Mater 1998;46:3893–904.
[19] Takaki Y, Masuda T, Kobayashi E, Sato T. Effects of natural aging on bake hardening behavior of Al-Mg-Si alloys with multi-step aging process. Mater Trans 2014;55:1257–65.
[20] Saga M, Sasaki Y, Kikuchi M, Yan Z, Matsuo M. Effect of pre-aging temperature on the behavior in the early stage of aging at high temperature for Al-Mg-Si alloy. Mater Sci Forum 1996;217:821–6.
[21] Fischer FD, Svoboda J, Appel F, Kozeschnik E. Modeling of excess vacancy annihilation at different types of sinks. Acta Mater 2011;59:3463–72.
[22] Liu M. Modulated clustering and precipitation in an Al–Mg–Si alloy AA 6014 via enhanced pre-aging. Acta Mater 2024. submitted to.
[23] Krause-Rehberg R. Positron annihilation in semiconductors. Heidelberg: Springer; 1999.
[24] Lang P, Shan YV, Kozeschnik E. The life-time of structural vacancies in the presence of solute trapping. Mater Sci Forum 2014;794–796:963–70.
[25] Hirosawa S, Nakamura F, Sato T. First-principles calculation of interaction energies between solutes and/or vacancies for predicting atomistic behaviors of microalloying elements in aluminum alloys. Mater Sci Forum 2007;561–565:283–6.
[26] Werinos M, Antrekowitsch H, Kozeschnik E, Ebner T, Moszner F, Löffler JF, Uggowitzer PJ, Pogatscher S. Ultrafast artificial aging of Al-Mg-Si alloys. Scripta Mater 2016:148–51.
[27] Zurob HS, Seyedrezai H. A model for the growth of solute clusters based on vacancy trapping. Scripta Mater 2009;61:141–4.
[28] Yan Y. Investigation of the negative and positive effects of natural ageing on artificial ageing response in Al-Mg-Si alloys, (Ph.D. thesis). TU Berlin; 2014.
[29] Jiang B, Wang HS, Yi DQ, Tian Y, Shen FH, Wang B, Liu HQ, Hu Z. Effect of Ag addition on the age hardening and precipitation behavior in an Al-Cu-Li-Mg-Zn-Mn-Zr alloy. Mater Char 2020;162:110184.
[30] Lang P, Falahati A, Povoden-Karadeniz E, Ahmadi MR, Warczok P, Kozeschnik E. Modeling of the yield strength evolution in Al-Mg-Si alloys. 12th international conference on aluminium alloys. Japan: Yokohama; 2010.
[31] Myhr OR, Grong Ø, Andersen SJ. Modelling of the age hardening behaviour of Al–Mg–Si alloys. Acta Mater 2001;49:65–75.
[32] Esmaeili S, Lloyd DJ, Poole WJ. Modeling of precipitation hardening for the naturally aged Al-Mg-Si-Cu alloy AA6111. Acta Mater 2003;51:3467–81.
[33] Song M. Modeling the hardness and yield strength evolutions of aluminum alloy with rod/needle- shaped precipitates. Mater. Sci. Eng. A 2007;443:172–7.
[34] Deschamps A, Brechet Y. Influence of predeformation and ageing of an Al-Zn-Mg alloy—II. Modeling of precipitation kinetics and yield stress. Acta Mater 1999;47:293–305.
[35] Esmaeili S. Precipitation hardening behaviour of AA6111. University of British Columbia; 2002. Ph.D. thesis).
[36] Gerold V. Dislocations in solids. North Holland, Amsterdam: North-Holland Publishing Company; 1979.
[37] Panseri C, Federighi T. A resistometric study of pre-precipitation in an aluminium-1.4% Mg_2Si alloy. J Inst Met 1966;94:99–197.
[38] Marioara CD, Andersen SJ, Hell C, Frafjord J, Friis J, Bjørge R, Ringdalen IG, Engler O, Holmestad R. Atomic structure of clusters and GP-zones in an Al-Mg-Si alloy. Acta Mater 2024;269:119811.
[39] Li ZG, Zhao PZ, J ZH, Liu ZS, Xie ZQ. Effects of Mg and Si contents on the microstructure and mechanical properties of AA6014 alloys in T4P and T6P temper. Mater. Sci. Eng. A 2019;740–741:187–200.
[40] Lomer WM. Vacancies and other point defects in metals and alloys. Inst. Metals 1958:79.
[41] Pogatscher S, Kozeschnik E, Antrekowitsch H, Werinos M, Gerstl SSA, Loffler JF, Uggowitzer PJ. Process-controlled suppression of natural aging in an Al-Mg-Si alloy. Scripta Mater 2014;89:53–6.
[42] Werinos M, Antrekowitsch H, Ebner T, Prillhofer R, Uggowitzer PJ, Pogatscher S. Hardening of Al-Mg-Si alloys: effect of trace elements and prolonged natural aging. Mater Des 2016;107:257–68.
[43] Werinos M, Antrekowitsch H, Ebner T, Prillhofer R, Curtin WA, Uggowitzer PJ, Pogatscher S. Design strategy for controlled natural aging in Al-Mg-Si alloys. Acta Mater 2016;118:296–305.
[44] Zhang XP, Liu M, Sun HM, Banhart J. Influence of Sn on the age hardening behavior of Al-Mg-Si alloys at different temperatures. Materialia 2019;8:100441.